REPORT DOCUMENTATION PAGE

Form Approved
OMB No. 0704-0188

1. AGENCY USE ONLY (Leave blank)	2. REPORT DATE	3. REPORT TYPE AND DATES COVERED
	March 1996	Final, 15 Aug 95 - 14 Feb 96

4. TITLE AND SUBTITLE

Preparation and Evaluation of Single-Crystal Yttrium Titanate-Based Monofilaments

5. FUNDING NUMBERS

F49620-95-C-0066

6. AUTHOR(S)

J.H. Sheehan, R.J. Prince and G.H. Reynolds, MSNW, Inc.
J.S. Haggerty and J. Sigalovski; MIT

AFOSR-TR-96 97

0020

7. PERFORMING ORGANIZATION NAME(S) AND ADDRESS(ES)

MSNW, Inc.
PO Box 865
San Marcos, CA 92079

9. SPONSORING/MONITORING AGENCY NAME(S) AND ADDRESS(ES)

Air Force Office of Scientific Research
AFOSR/NA
110 Duncan Ave, Suite B115
Bolling AFB DC 20332-8080

10. SPONSORING/MONITORING AGENCY REPORT NUMBER

11. SUPPLEMENTARY NOTES

12a. DISTRIBUTION/AVAILABILITY STATEMENT

Approved for public release, distribution is unlimited.

12b. DISTRIBUTION CODE

13. ABSTRACT (Maximum 200 words)

This SBIR Phase I research produced and characterized single-crystal monofilaments of Y2Ti2Oz for preliminary evaluation as reinforcement. These Experiments were initiated without benefit of prior experience with the material because no crystal growth citations were identified and equilibrium phase relationships were incomplete.

19970117 164

14. SUBJECT TERMS

Ceramic, Fiber, Yttrium Titanate, Monofilament

15. NUMBER OF PAGES

16. PRICE CODE

17. SECURITY CLASSIFICATION OF REPORT	18. SECURITY CLASSIFICATION OF THIS PAGE	19. SECURITY CLASSIFICATION OF ABSTRACT	20. LIMITATION OF ABSTRACT
UNCLASSIFIED	UNCLASSIFIED	UNCLASSIFIED	UNLIMITED

MSNW, Inc.
P.O. Box 865
San Marcos, CA 92079

PREPARATION AND EVALUATION OF SINGLE-CRYSTAL YTTRIUM TITANATE-BASED MONOFILAMENTS

Phase I SBIR Final Report

March 1996

Prepared For: Air Force Office of Scientific Research

Contract Number: F49620-95-C-0066

Prepared By: J.E. Sheehan, R.J. Price, and G.H. Reynolds, MSNW, Inc.
J.S. Haggerty and J. Sigalovsky,
Massachusetts Institute of Technology

TABLE OF CONTENTS

INTRODUCTION

Thermochemically stable, high strength, high thermal expansion coefficient monofilaments are required for reinforcing a variety of titanium alloy and titanium intermetallic composite matrices. Experience with other reinforcements suggests that thermochemical stability is primarily related to composition while strength and damage tolerance are mostly defined by crystal structure. A review of alternative materials identified, heretofore unexplored, yttrium titanate pyrochlore ($Y_2Ti_2O_7$) as one of the more interesting candidate materials for reinforcement of titanium-based matrices. A large and complex unit cell is expected to give $Y_2Ti_2O_7$ elevated temperature mechanical properties that are superior to those of c-axis sapphire. When equilibrated in reducing conditions, $Y_2Ti_2O_7$ is expected to be thermochemically stable in a range of titanium alloy and titanium aluminide matrices. Also, its estimated thermal expansion coefficient is expected to be higher than those of other refractory oxides and quite close to those of titanium aluminides.

This Phase I research produced and characterized single-crystal monofilaments of $Y_2Ti_2O_7$ for preliminary evaluation as reinforcements. These experiments were initiated without benefit of prior experience with the material because no crystal growth citations were identified and equilibrium phase relationships were incomplete.

APPROACH AND PROCEDURES

Filament growth experiments were conducted using the CO_2 laser-heated floating-zone process (LHFZ) because it is ideally suited for exploring accessible properties of new monofilaments (Figure 1) (Refs. 1,2). In this process, the melt zone is supported by surface tension between the feed rod and the growing fiber; the melt is formed from heat absorbed by a focused CO_2 laser heat source. A properly oriented seed crystal is brought into contact with the molten zone to produce a single-crystal filament of the desired orientation in the final pull.

The two controlled atmosphere LHFZ units that were used at MIT to produce the monofilaments are shown in Figure 2. The first unit, which employs a 1500 watt 2-beam CO_2 laser with optics for 4-beam heating, was used to reduce feed rods from the 3.5 mm starting diameter to about 0.8 mm in three runs. The second unit employed a 1500 watt CO_2 laser with 2-beam optics and was used to grow the final filaments with diameters of 0.15 to 0.20 mm (150 to 200 μm) in two pull runs using the 0.8 mm material as feed. Temperature measurements were made during growth and compared with crystal and zone compositions to derive information about the phase diagram which is virtually nonexistent for the Y_2O_3-TiO_2 binary in the vicinity of the $Y_2Ti_2O_7$ melting point (Figure 3) (Ref. 3).

Feed rods for the LHFZ process were sawed from cold pressed and sintered disks. Powder lots of two types were made using a high-purity Y_2O_3 sol and two TiO_2 powders. One type was made from TiO_2 containing about 2 wt % Al_2O_3 and the other from a high-purity TiO_2 grade. The two methods can be described as follows:

1. Preparation from Kronos Pigment Grade Titania and PQ Colloidal Yttria

The two starting materials were Kronos 2020 pigment grade titania and colloidal yttria (PQ Corporation). The pigment grade titania is an alumina coated powder with a particle size of about 300 nm. The overall composition is 94% titania and 6% alumina. The yttria sol contains 10 nm yttria particles. The two starting materials were combined. The slurry was then dried with stirring and dry milled. The powder was calcined at 800°C, pressed, and fired to 1300°C in air to densify it.

2. Preparation from NanoTek Titania and PQ Colloidal Yttria

The two starting materials were NanoTek titania and colloidal yttria (PQ Corporation). The NanoTek titania is a powder with a particle size of about 30 nm. The yttria sol contains 10 nm yttria particles. The two starting materials were combined. The sol was dried with stirring and then dry milled. The powder was calcined at 1050°C, pressed, and fired to 1300°C in air to densify it.

Feed rods received by MIT were characterized by x-ray diffraction to identify phases and measure the $Y_2Ti_2O_7$ lattice parameter, and physically to determine the fractional density. Feed rods made using the impure TiO_2 were brown and had high concentrations of dark spots. SEM microphotographs of Figure 4 showed that the spots were cavities with small crystals grown on the cavity surfaces. Optical microscopy revealed that the crystals on the cavity surfaces were dark in color. Detailed EDX analysis of Figure 4 revealed that the crystals contained high concentrations of either Al or Fe. Later rods made of the same starting materials, but sintered at a lower temperature, were white and did not have spots. Rods made using the pure TiO_2 were also white and spotless.

Lattice parameters of the $Y_2Ti_2O_7$ phase in the feed rods were generally within the range of those reported in the literature. Lattice parameters exhibited significant variations between individual lots as well as between feed rods taken from the same lot. As will be shown in more detail in the monofilament growth section, the $Y_2Ti_2O_7$ lattice parameter appears to be related to the Ti content.

Densities of the feed rods were in the range of 35-45% of theoretical (4.99 $g \cdot cm^{-3}$) and varied from lot to lot and between rods taken from the same lot. Characteristics of the feeds are summarized in Table 1.

Table 1. Summary of Feed and Monofilament Characteristics

Sample Designation	Color	Prior Temp (°C) S/M	Lattice Parameter (Å)	Standard Deviation (Å)	Composition by XRD				Impurities by ESEM/EDX
					$Y_2Ti_2O_7$	TiO_2 rutile	Y_2O_3	Other phases	
Feed 1-1 (impure)	Beige, dark spots	1,400 (S)	10.0922	0.0005	VS	W	-	W: u/i-1, VW:u/i-2	Fe, Al
IX-9-2 fiber	Dark red-brown		10.1000	0.0007	VS	-	-	-	
Feed 1-3 (impure)	Beige	1,400 (S)	10.0934	0.0002	VS	-	-	VW: u/i-2	
IX-13-2 [110]	Red-brown		10.0992	0.0004	VS	-	-	-	
IX-27-2 (grown from 2-2) (impure)	Brown				VS	-	-	-	
Feed 3-2 (pure)	White	1,400 (S)	10.0954	0.0004	VS	W	W	W: u/i-3	
VIII-44-1/1 steady	Brown	2,100 (M)	10.0983	0.0011	VS	T	-	-	
VIII-44-1/1 quen.zone		2,100 (M)	10.0972	0.0006	VS	W	-	-	
IX-20-1 fiber	White		10.0942	0.0004	VS	-	-	-	
IX-19-1 fiber	Brown		10.0972	0.0005	VS	-	-	-	
Feed 5-1 (impure)	White	1,300 (S)	10.0920	0.0010	VS	-	-	VW: u/i-2	
IX-32-2	Light brown		10.1095	0.0007	VS	-	-	-	
From literature:									
JCPDS file 42-0413 (1991)	White		10.0947	0.0002					
Becker&Will (1969)			10.0980	0.0050					
Becker&Will (1970)			10.0896	0.0014					

X-ray Intensities: VS = very strong (phase with the 100% intensity peak)
W = weak (the largest peak = ~5-10% of the major phase largest peak)
VW = very weak (the largest peak = ~1-5% of the major phase largest peak)
T = trace (the largest peak < 1% of the major phase largest peak)
u/i = unidentified phase

Designations S = sintered
M = melted

Feed Sample Code: The first number designates the disk number and the second corresponds to the sample cut from the disk

Process variables explored for growth of $Y_2Ti_2O_7$ include feed rod processing history, monofilament growth atmosphere, crystallographic growth direction, monofilament diameter, and pulling rate. The ranges of conditions used for approximately 67 growth runs are summarized in Table 2. Crystals were grown either in air or in pure O_2 atmospheres. Monofilament growth runs were initiated both from polycrystalline rods and from precisely oriented seed crystals having [111], [110], or [311] orientations. Monofilaments were all pulled in a downward direction; intermediate pulls were made in a combination of upward and downward pulls that were otherwise identical and indistinguishable. Monofilament diameters ranged from 250 to 400 μm, and pulling rates ranged from 2 to 15 cm/h. The pull-to-feed speed ratio was varied from 1/1 to 10/1. For these experiments, 4 to 8 zone meltings were required to reduce diameters to desired monofilament dimensions. Monofilaments grown for mechanical tests were grown in O_2 at 10 cm/h in the [111] and [311] directions.

Room temperature tensile strengths were measured with a table-top single filament tester (Figure 5) using the epoxy tab technique to align the monofilaments in the grips in a manner consistent with ASTM D3379-75. Room temperature tensile strengths were measured with a 6.4 mm gage length and a cross head travel rate of 1 mm/min. If monofilaments satisfying minimum room temperature strengths (>2 GPa) were obtained, it was planned to further evaluate such monofilaments by high temperature delayed failure tests and by short term tensile strength tests at 1200°C.

Chemical compatibility was assessed by incorporating multiple short lengths of $Y_2Ti_2O_7$ monofilaments into titanium alloy and titanium intermetallic matrices having a range of Ti activities (in decreasing order: Pratt & Whitney Alloy C (a Ti-Cr-V beta alloy), α-2, and orthorhombic) by vacuum hot pressing of monofilament-powder mixtures. The product composites were sectioned, mounted and polished for photomicrographic examination and SEM/x-ray analysis identification of any interfacial chemical reactions.

Table 2. Summary of $Y_2Ti_2O_7$ Monofilament Growth Experiments, Run Conditions and Observations

Pull No.	Crystal Grower	Run No.	Feed Rod	Pick up	Atmosphere	Pressure (psig)	Total Beam Power (W)	Laser Spot Size (mm)	Shaft Speeds (cm/hr) Upper Head	Shaft Speeds (cm/hr) Lower Head	Rotation (rpm) Upper Head	Rotation (rpm) Lower Head	Growth axis [hkl]	Diameter of Grown Crystal (mm)	Comments
1	P1003	VIII-37-1	Feed #1-1a	Feed #1-1b	Air	0	120	3	4	4	18	8	spont. [311]		Stable melt, bubbles, crystal is cracked, non-uniform diameter
2		VIII-37-1/1	VIII-37-1	Feed #1-1a	Air	0	110	3	4	2.74	18	-	direction#2		Stable melt, not uniform diameter
3		VIII-37-1/2	VIII-37-1/1	VIII-37-1	Air	0	80	3	2.4	4	-	29	[311]		Stable melt, not uniform diameter
4	P108	IX-9-1	VIII-37-3	VIII-37-1/1	Air	0	48.2	1.2	1.53	10	-	-	direction#2		
5		IX-9-2	IX-9-1	VIII-37-3	Air	0	24.7	1.2	1.5	10	-	-	[311]		
1	P1003	VIII-40-1	Feed #1-2	VIII-37-1/1	Air	0	180	3	4.47	4	8	18	direction#2	2.54	Bubbles, crystal is cracked, not uniform dia., stable melt.
2		VIII-40-1/1	VIII-40-1	Feed #1-2	Air	0	130	3	4	2.74	8	18	spont. [311]	2.10	Not uniform diameter, stable melt.
3		VIII-40-1/2	VIII-40-1/1	VIII-40-1	Air	0	90	3	2.74	4	8	-	direction#2	1.74	Tmelt.= 2050 Tsolidif.= 2040, T peak=2180°C
4		VIII-40-1/3	VIII-40-1/2	VIII-40-1/1	Air	0	65	3	4	3.13	8	15	[311]	1.54	
5	P108	IX-10-1	VIII-40-1/3	VIII-40-1/1	Air	0	42.0	1.2	2.1	10	-	-	[311]	0.70	
5		IX-13-1	VIII-40-1/3	IX-10-1	Air	0	43.1	1.2	2.16	10	-	-	[111]	0.71	
6		IX-13-2	VIII-40-1/3	IX-10-1	Air	0	38.3	1.2	1.76	10	-	-	[110]	0.65	
1	P1003	VIII-41-1	Feed #1-3a	VIII-37-1/1	Air	0	180	3	4	4	8	18	direction#2	2.5	Bubbles, crystal is cracked, not uniform dia., stable melt.
1		VIII-41-2	Feed #1-3b	VIII-41-1	Air	0	190	3	4	4	8	18	direction#2	2.5	Not uniform diameter, stable melt.
2		VIII-41-2/1	VIII-41-2	Feed #1-3b	Air	0	130	3	4	2.74	15	18	direction#4	2.07	Tmelt=2062, Tsolidif.= 2060, Tpeak=2155°C
3		VIII-41-2/2	VIII-41-2/1	VIII-41-2	Air	0	90	3	8.18	9.95	8	18	direction#2	1.9	
4		VIII-42-1	VIII-41-2/2	VIII-41-2/1	Air	0	90	3	6	4.69	8	8	direction#4	1.68	
5		VIII-42-2	VIII-42-1	VIII-42-1	Air	0	90	3	4	4	8	8	direction#4	1.68	
6	P108	IX-14-1	VIII-42-2	VIII-40-1/1or2	Air	0	53.6	1.2	2.5	10	-	-	?	0.84	
7		IX-14-2	IX-14-1	IX-13-1	Air	0	29.4	1.2	3.09	10	-	-	[111]	0.47	
7		IX-14-3	IX-14-1	IX-13-1	Air	0	32.6	1.2	3.09	10	-	-	[111]		
8		IX-15-1	IX-14-2	IX-14-3	Air	0	15.4	1.2	4.89	10	-	-	[111]		
8		IX-16-1	IX-14-2	IX-10-1	Air	0	16.7	1.2	1.6	10	-	-	[311],[111]	0.18	
1	P1003	VIII-43-1/1	Feed #3-2a	Feed #3-1	Air	0	185	3	4	4	7.7	7.7	direction #5	2.63	Melt is not stable, jumps up and down and boils.
2		VIII-43-1/2	Feed #3-1	VIII-43-1/1	Air	0	180	3	4	4	7.7	7.7	direction #6	2.63	Melt is not stable, jumps up and down and boils.
3		VIII-43-1/3	VIII-43-1/2		O2	0	140	3	4	2.74	7.7	7.7	direction #5a	2.18	Tp = 2200-2218; Tm = 2060-2080; Ts = 2070-2080
4		VIII-44-1/1	VIII-43-1/3	VIII-43-1/2	O2	0	100	3	2.7	4		7.7	direction #6	1.8	Melt is jumping. Tpeak = 2190; Tsolidific. = 2100
5		VIII-44-1/2	VIII-44-1/1	VIII-43-1/3	O2	0	80	3	4	2.3	11.1		direction #5a	1.38	Quenched zone at the end
1	P1003	VIII-45-1/1	Feed #3-2b	Feed #3-3	O2	0	175	3	4	4	7.7	7.7	direction #7	2.6	Relatively stable melt.
1		VIII-45-1/2	Feed #3-3	Feed #3-2b	O2	0	170	3	4	4	7.7	7.7	direction #8	2.6	Melt is not stable, jumps up and down.
2		VIII-45-2	VIII-45-1/2	Feed # 3-3	O2	0	150	3	4	2.74	7.7	7.7	direction #7a	2.18	
3		VIII-45-3	VIII-45-2	VIII-45-1/2	O2	0	110	3	3.03	5.86	7.7	7.7	direction #8	1.57	Tpeak= 2175°C, Tmelt= 2100°C, Tsolidific.= 2120°C
4		VIII-46-1	VIII-45-3	VIII-45-2	O2	0	270/4	3	5.94	2.93	7.7	7.7	direction #7a	1.1	Choppers on the laser beams
5		VIII-46-2	VIII-46-1	IX-14-1	O2	0	200/4	3	2	6			[311]	0.64	
6	P108	IX-18-1	VIII-46-2	IX-16-1	O2	0	20.3	1.2	2.34	10			[311]	0.31	Melt moves up and down for 1/2 zone length
7		IX-19-1,20-1	IX-18-1	IX-16-1	O2	0	13.7	1.2	2.34	10			[311]	0.15	After ~4cm, xtal changed direction to [111]
6		IX-20-2	VIII-46-2	IX-18-1	O2	0	23.4	1.2	0.5	2			[311]	0.32	
7		IX-20-3	IX-20-2	IX-9-2	O2	0	15.8	1.2	0.5	2			[311]	0.16	Strong diam. variables

Table 2. Summary of $Y_2Ti_2O_7$ Monofilament Growth Experiments, Run Conditions and Observations (Continued)

Pull No.	Crystal Grower	Run No.	Feed Rod	Pick up	Atmosphere	Pressure (psig)	Total Beam Power (W)	Laser Spot Size (mm)	Shaft Speeds (cm/hr) Upper Head	Shaft Speeds (cm/hr) Lower Head	Rotation (rpm) Upper Head	Rotation (rpm) Lower Head	Growth axis [hkl]	Diameter of Grown Crystal (mm)	Comments
1	P1003	VIII-47-1/1	Feed #1-1a	Feed #1-1b	O2	0		3	4	4	7.7	7.7	direction #9	~3 mm	Very stable melt.
2		VIII-47-1/2	Feed #1-1b	VIII-37-1/3	O2	0		3	2.83	4	7.7	7.7	[311]	2.5	Very stable melt
3		VIII-47-1/3	VIII-47-1/2	Feed #1-1b	O2	0		3	4	2.35	7.7	7.7	direction #9	1.9	Very stable melt
4		VIII-47-1/4	VIII-47-1/3	VIII-47-1/2	O2	0		3	2.42	4	7.7	7.7	[311]	1.5	Very stable melt
5		VIII-48-1	VIII-47-1/4	VIII-37-3	O2	0	280/4	3	4	1	7.7		[311]	0.75	Very stable melt. With choppers
6	P108	IX-24-1	VIII-48-1	IX-9-2	O2	0	20.9	1.2	1.14	4			[311]	0.4	
7		IX-24-2	IX-24-1	IX-9-2	O2	0		1.2	1.4	10			[311]	0.15	Very hard to start, xtal separates
7		IX-25-1	IX-24-1	IX-9-2	O2	0		1.2	1	4			[311]	0.2	Not stable, did not grow
6		IX-25-2	VIII-48-1	IX-9-2	O2	0	23.9	1.2	1.14	4				0.4	To keep zone const. power needed to be changed
1	P1003	VIII-48-2	Feed #2-1a	Feed #2-1b	O2	0	180	3	4	4	7.7	7.7	direction #10	2.14	Stable melt.
2		VIII-49-1	VIII-48-2	Feed #2-1b	O2	0	400/4	3	4	1.25	7.7	7.7	direction #11		With choppers
3		VIII-49-2	VIII-49-1	VIII-48-2	O2	0	290/4	3	1	4			direction #10		Xtal is cracked, non-uniform diam.
3		VIII-49-3	VIII-49-1	VIII-46-2	O2	0	270/4	3	1	4			[311]		Xtal is cracked, non-uniform diam.
4	P108	IX-26-1	VIII-49-3	IX-25-1	O2	0	19.2	1.2	1	4			[311]	0.295	
1	P1003	VIII-50-1/1	Feed #2-2	VIII-37-1/3	O2	0	400	3	2	4	7.7	7.7	[311]	2.47	Stable melt.
2		VIII-50-1/2	VIII-50-1/1	Feed #2-2	O2	0	150	3	4	1	7.7	7.7	direction #12	1.75	
3		VIII-50-2	VIII-50-1/2	VIII-50-1/1	O2	0	350-400/4	3	1	4			[311]	0.875	With choppers
4	P108	IX-26-2	VIII-50-2	IX-9-2	O2	0	31.3	1.2	1.88	4			[311]	0.6	
5		IX-27-1	IX-26-2	IX-24-1	O2	0	18.2	1.2	1	4			[311]	0.283	
5		IX-27-2	IX-26-2	IX-27-1	O2	0	17.4	1.2	1	4			[311]	0.3	Fiber separated from the melt
5		IX-31-1	IX-26-2	IX-16-1	O2	0	20.5	1.2	2.5	10			[111]	0.3	Triangular shape, steps on flat faces
1	P1003	VIII-51-1/1	Feed#2-3	VIII-37-1/3	O2	0	400	3	2	4	7.7	7.7	[311]	3.05	Satble melt.
2		VIII-51-1/2	VIII-51-1/1	Feed#2-3	O2	0	230	3	4	1	7.7	7.7	direction#13	2.16	Tmelt=2030, Tpeak=2090, Tsolidif.=2010
3		VIII-51-2	VIII-51-1/2	VIII-51-1/1	O2	0	400/4	3	1	4			[311]	1.08	W/choppers. Cracks, non-uniform diameter.
4	P108	IX-32-1	VIII-51-2	IX-26-2	O2	0	31.5	1.2	4	~1			[311]	0.56	Feed rate correction based on current feed diam.
5		IX-32-2	IX-32-1	IX-16-1	O2	0	21.1	1.2	~2.5	10			[111]	0.28	Feed rate correction based on current feed diam.
4		IX-33-1	VIII-51-2	IX-32-1	O2	0	33.8	1.2	4	~1			[311]	0.54	Feed rate correction based on current feed diam.
5		IX-33-2	IX-33-1	IX-16-1	O2	0	21.4	1.2	~2.5	10			[111]	0.27	Feed rate correction based on current feed diam.
4		IX-35-1	VIII-51-2	IX-32-1	O2	0	33.5	1.2	4	~1			[311]	0.56	Feed rate correction based on current feed diam.
5		IX-35-2	IX-35-1	IX-16-1	O2	0	17.2	1.2	~2.5	10			[111]	0.28	
1	1003	VIII-52-1	Feed #5-1	VIII-51-2	O2	0	160	3	2	4	7.7	7.7	[311]	1.58	White color. Bubbles.
2		VIII-53-1	VIII-52-1	Feed #5-1	O2	0	460/4	3	15	3.75	7.7		direction#14	1.12	Stable melt.
3	P108	IX-36-1	VIII-53-1	IX-32-1	O2	0	37.2	1.2	4	~1			[311]	0.56	Melt is very stable, no visible cracks
4		IX-36-2	IX-36-1	IX-16-1	O2	0	20.2	1.2	~2.5	10			[111]	0.28	Feed rate correction based on current feed diam.

Thermal expansion coefficients were measured between room temperature and 1000°C using a fused silica dilatometer. Monofilament samples were 2.5 cm long.

RESULTS AND DISCUSSION

Feed Rods

Feed rods made from the first two disks (less pure ingredients) were brown and had high concentrations of dark spots. EDX analysis revealed that the crystals surrounding the dark spots contained relatively high concentrations of Al (impurities in feed) or Fe (milling contaminant). Disk 5 made of the same starting materials, but sintered at the lower temperature, was white and did not have spots. Disks 3 and 4, produced from pure reactants, were also white and spotless. Densities of feed rods cut from the disks varied from disk to disk in the range of 35-45% of theoretical.

X-ray diffraction analysis showed that phase contents of the feeds varied from disk to disk and between feed rods cut from the same disk (Table 1). Feed 1-1 contains rutile as the second phase, while neither feed 1-3 (from the same disk) nor feed 5 exhibits rutile peaks. Disk 3 made of pure reactants contains both free TiO_2 and Y_2O_3. In addition to these major phases, trace levels of three still unidentified phases were found in combinations reported in Table 1. Low intensities of the few detectable peaks did not permit reliable identifications of these minor phases; it was determined that none of the known phases in the systems Y-Ti-O or Fe-Al-O fits these peaks.

Lattice parameters of the $Y_2Ti_2O_7$ phase in the feeds are generally within the range of those reported in the literature (Refs. 4-6) (Figure 6). They also exhibit significant variations (more than an order of magnitude larger than the standard deviations) between individual disks as well as between feed rods cut from the same disk. As will be shown in more detail in the monofilament growth section, the $Y_2Ti_2O_7$ lattice parameter appears to be related to the Ti content.

Crystal Growth

The $Y_2Ti_2O_7$ material easily satisfied fundamental requirements for LHFZ monofilament growth. Quiet, non-volatile melts were formed on polycrystalline feed rods as well as between feeds and growing crystals in air and in O_2. Also, melt dimensions could be precisely controlled with the laser power levels.

The $Y_2Ti_2O_7$ material also satisfied more stringent requirements needed for growing single-crystal monofilaments. Single-crystals were produced with virtually all employed growth conditions. With the exception of one intermediate crystal, powder x-ray diffraction analysis showed all zone melted material to be single phase $Y_2Ti_2O_7$. Crystals that were grown from polycrystalline pickups usually grew along an axis that was within 4-7° of a [311] axis. When growth was initiated from [111] or [311] seeds, the crystals usually assumed the crystallographic orientations of the seeds and maintained seeded axes for lengths up to 10-30 cm. Except for the [110] monofilaments, Laue x-ray diffraction patterns of zone melted material gave sharp spot patterns with spot sizes corresponding to the illuminated dimensions; there was no evidence of spot distortion or splitting which result from low angle boundaries. For still unexplained reasons, all attempts to produce [110] monofilaments yielded material that was so faulted that it was effectively polycrystalline.

Melt zone lengths were more sensitive to laser power than is true for sapphire monofilaments. In contrast, melt zone lengths appear to be less sensitive to factors which control heat losses through the monofilament and the feed rod than is true of sapphire. Both characteristics are consistent with $Y_2Ti_2O_7$ having a low thermal conductivity, as would be expected for a material having a large complex unit cell containing elements with dissimilar masses.

Rods produced by zone melting were usually cracked when diameters were larger than 800 μm. Occasional cracks were usually evident in 600 μm intermediates,

but none were observed for diameters less than 500 μm. It is probable that residual stress cracking results from the combination of high thermal expansivity and low thermal conductivity Polymorphic phases, a common alternative source of stress, were not evident in this compound.

Problems also were evident. Single-crystals of $Y_2Ti_2O_7$ exhibited such a strong propensity to develop surface facets on multiple planes that process control was compromised and monofilament strengths were diminished. Two difficulties arise if the pulling axis does not lie within facet planes on surfaces of growing monofilaments. The first caused the monofilaments to become crooked (bent or hooked) on a length scale corresponding to a few monofilament diameters as the localized growth axis alternated between directions lying in competing facet planes. This off-axis growth occurred for appreciable distances because the monofilaments were so compliant that they could not force growth to follow the pulling axis. Localized growth directions and solidification rates both change discontinuously as the dominant facet changes. The second problem resulted because the zone volume changed significantly as individual facets appeared and disappeared. Non-uniform solidification rates and zone volumes both cause localized compositional variations in the solidifying material. Reductions in strength result from stress concentrations at the sharp intersections between competing facet planes. Also, rough faceted surfaces impede monofilaments from sliding in a matrix.

Varying melt dimensions resulting from faceting effects frequently caused the zone to pinch off when growth was attempted with normal pull-to-feed speed ratios (9/1-10/1). Consequently, most growth was conducted with pull-to-feed speed ratios around 4/1 because these zone shapes are more robust to the effects of perturbations and because the resulting monofilaments have larger diameters and are stiffer, thus are more resistant to off-axis growth.

These faceting problems experienced for $Y_2Ti_2O_7$ are similar to problems that have been successfully resolved with both a-axis sapphire and spinel ($MgO{\cdot}Al_2O_3$) monofilaments by precisely aligning the pulling axes with the facet planes (Ref. 7).

Implementing the oriented growth axis strategy depends on identifying the indices of facet planes observed on single-crystal surfaces. Monofilaments grown along [311] axes at low rates exhibited large macroscopic facets like those shown in Figure 7. In contrast, monofilaments grown relatively rapidly (~10 cm/h) along a [111] axis from some specific seed crystals exhibited smooth, nominally triangular cross sections [Figure 8(a)]. The [111] monofilaments were emphasized because they appeared smoother than other orientations and this is the favored stress axis for probable slip systems.

Although the cross sections of [111] monofilaments, like those in Figure 8(a), are distorted into a triangular shape, the bounding surfaces are curved rather than being flat facet planes as formed on other orientations. Laue analysis showed that the chords between the triangle's "points" were perpendicular to <211> axes in these [111] single-crystal monofilaments. Microstructural analysis of other single-crystal monofilament materials, which have exhibited non-circular cross sections bounded by macroscopically curved surfaces, has usually shown that the curvature results from a set of 2, or more, microscopic, flat, facet planes working in combination. The orientation strategy can work successfully even for these monofilaments because the macroscopic curvature usually results from continuously varying the dimensions of the facet planes making up the set, analogous to varying the rise and run on a stair. Ideally the facet planes making up the set all lie parallel to the selected growth axis. If made fine enough, high monofilament strengths can be achieved even if one of the facet planes in the set does not lie exactly parallel to the growth axis.

Uncoated samples of [111] monofilaments grown at higher rates were examined at magnifications up to 28,500X using an environmental SEM microscope. Contrary to

experience with other materials, the surfaces of these single-crystal monofilaments never exhibited distinguishable facet planes. Coarse and fine features, like those shown in Figures 8(b)-8(c), were evident at all levels of magnification. Observations at higher levels of magnification simply revealed new sets of similar small-scale features [Figure 8(d)].

Two phenomena correlated with the severity of macroscopic faceting. Monofilaments which were colorless were much more strongly faceted than those which were dark. Monofilaments originating from feeds cut from disks 1, 2, and 5 were always very dark. Monofilaments originating from disk 3 alternated between dark and clear along their lengths. Second, melt zones formed from disks 1 and 2 were quiet and clear, while melt zones formed from disk 3 exhibited continuously swirling light and dark regions having dimensions on the scale of the zones. Monofilaments grown from the swirling zones were much more faceted than the others. Growth from disk 5 was very similar to disk 3 until the [311] growth rate was increased from 4 to 15 cm/h. Subsequent [111] monofilament growth from a rapidly pulled [311] intermediate diameter feed was very stable and free of faceting effects even at low rates. Past experience with other materials suggests that the swirling patterns in the melt zones may result from having a 2-phase (solid and liquid) zone.

Observed phases and lattice parameters reported in Table 1 were compared with observations about growth and monofilament characteristics. With repeated meltings, multiphase feeds yielded single-phase crystals. Unidentified (minor) phases in the feeds were not observed in any of the melted samples. Because there is no apparent weight loss during growth, the emergence of single-phase material indicates that the initial feeds have a composition lying within the single-phase $Y_2Ti_2O_7$ field that is accessible by melt processing. The disappearance of phases other than $Y_2Ti_2O_7$ results from homogenization during melting. Based on the formulations of the feed rods, the results also show that the high temperature single-phase $Y_2Ti_2O_7$ field includes the stoichiometric composition.

The zone quenched from the intermediate crystal (feed 3) contains more free TiO_2 than the crystal, showing that Ti is segregated into the zone during growth. This result indicates that the liquidus composition from which this crystal grew lies on the TiO_2 side of the solidus which bounds the $Y_2Ti_2O_7$ phase field.

The coexistence of single-phase $Y_2Ti_2O_7$ with varying quantities of TiO_2 and Y_2O_3 phases in samples having constant overall compositions indicates that single-phase $Y_2Ti_2O_7$ exists with a range of Y/Ti ratios that should be reflected by changing lattice parameters. Based on the phase analyses, it is probable that the $Y_2Ti_2O_7$ phases in the melted material contain more Ti than the sintered feeds. With the exception of the monofilament grown from feed 3, lattice parameters in the monofilaments exceeded those of the $Y_2Ti_2O_7$ phase in the sintered feed rods from which they originated. These observations indicate that higher Ti concentrations result in larger lattice parameters.

The lattice parameter results correlate with other observations. As shown in Table 2, temperatures measured at the solidification interfaces (solidus) for crystals grown from feed 3 (2070° - 2120°C) exceed those grown from the other type of feeds (1 and 5) (2010° - 2060°C). Also, monofilaments grown from feed 3 had smaller lattice parameters than those grown from other feeds, suggesting that the overall composition of the feed was deficient in TiO_2. These results are consistent with earlier conclusions about the relative compositions of the solidus and liquidus. They also indicate that all of the compositions lie to the TiO_2 rich side of the congruent melting composition.

It is probable that color reflects the Ti oxidation state rather than impurity levels since dark and light regions are observed along a single monofilament grown from feed 3, and also the discoloration disappears with flame polishing. Based on usual trends, Ti^{+4} probably does not introduce a color center while Ti^{+3} does; also Ti^{+4} is smaller than Ti^{+3}. As is observed in Figure 6, white monofilaments should have smaller lattice

parameters than dark monofilaments. Because impurities impact the Ti valence state, further characterizations are needed.

Neither the reasons for the discoloration of the monofilaments nor for the absence of microscopic facets on the [111] monofilaments have been resolved. Much still needs to be learned about growing single-crystal $Y_2Ti_2O_7$ monofilaments.

Mechanical Properties

Tensile strength measurements at room temperature confirmed the fragility originally observed in handling the monofilaments. Tensile strength results are summarized in Table 3. Monofilaments were tested in the as-produced condition. Selected specimens were also tested after annealing at 1300°C for 100 h in air, or after flame polishing. The maximum and minimum tensile strengths (σ_f) were 595 and 50 MPa, respectively.

The tensile strengths tend to show a wide scatter. There is no clear and systematic dependence of tensile strength on the feed rod used or on the growth direction. One [311] specimen and one [111] specimen were annealed in air at 1300°C for 100 h and replicate test specimens prepared. The [111] specimens showed a 56% increase in tensile strength after annealing over unannealed specimens from the same monofilament. No unannealed control specimens from the same monofilament were tested from the [311] monofilament that was annealed, but the mean strength of the annealed specimens was 200% higher than [311] specimens from a different monofilament produced from a different feed rod. These results suggest residual stresses are at least contributing to the low measured tensile strengths.

Monofilament samples originating from feed 5 were tested in the as-produced condition and also flame polished and tested. Although flame polishing enhanced development of surface facets and caused the dark discoloration to disappear, the

Table 3. Room Temperature Strengths of $Y_2Ti_2O_7$ Monofilaments

Sample Origin	Growth Direction	Filament Number	Diameter (μm)	Treatment	Strength (ksi)	Strength (MPa)
Feed 1b	[311]	1X-25-2	400	As grown	14.4 14.1	99 97
Feed 2-1a	[311]	1X-26-1	295	Annealed at 1300°C, 100 h	44.8 37.1 47.3	309 256 326
Feed 2-2	[111]	1X-31-1	300	As grown	17.4 23.4 17.2 9.0	120 161 119 62
Feed 2-2	[111]	1X-31-1	300	Annealed at 1300°C, 100 h	21.7 30.3	150 209
Feed 2-3	[111]	1X-33-2	270	As grown	32.5 51.0	224 352
Feed 2-3	[111]	1X-35-2	280	As grown	55.9 86.3	386 595
Feed 5-1	[111]	1X-36-2	280	As grown	34.6 52.0	239 359
Feed 5	[111]	1X-37-2	280	As grown	25.1 14.8 16.8 7.3 10.9	173 102 116 50 75
Feed 5	[111]	1X-37-2	280	Flame polished	16.0 (mean of 2)	110 (mean of 2)

flame polishing treatment had no measurable effect on tensile strength relative to the as-produced monofilaments.

The observed tensile strengths do not show an obvious dependence on the wide range of surface conditions investigated (macroscopic facets on [311], non-faceted as-grown [111], flame polished [111]). Unfortunately, mean strengths were nearly an order of magnitude lower than were sought before initiating high temperature tests. Using estimated values for the Young's modulus (E) and fracture surface energy (γ) of $Y_2Ti_2O_7$, 345 GPa and 17.5 J/m^2, respectively, the dimensions of the strength controlling flaw (C) in a 25 ksi (172 MPa) specimen were estimated from $\sigma_f \approx (E \cdot \gamma / 2C)^{1/2}$. This calculation indicates that strength controlling flaws had dimensions on the order of 100 μm, corresponding to 1/4 to 1/3 of the monofilament diameters. Fractography of tensile samples indicated that many fractures originated from internal flaws rather than the more typically observed (for single-crystal oxide monofilaments) surface flaws. As shown in Figure 9 for specimen No. 1X-25-2, an exceptionally low strength material, identified flaws were ≈100 μm diameter circles located on the monofilament centerlines. The location and dimensions of the fracture origins agree reasonably well with calculations and would explain the insensitivity of the tensile strength to surface conditions.

After annealing in air at 1300°C for 100 h, similar orientation monofilaments showed significantly higher strengths as noted above. Figure 10 shows the fracture surface of specimen No. 1X-26-1 where the fracture origin is clearly surface-connected and appears to be about 30 μm in dimension, which is consistent with the higher strength observed.

Monofilaments of a [111] growth direction often showed fracture surfaces which were almost featureless in the as-produced condition as shown in Figures 11, 12, and 13 for specimen Nos. 1X-37-2-3, 1X-33-2, and 1X-36-2, respectively. After annealing at 1300°C for 100 h, the single fracture surface studied appeared to exhibit a fracture

originating at porosity at the centerline of the monofilament as shown in Figure 14 for specimen No. 1X-31-1.

The origin of the strength controlling flaws has not been identified. High levels of residual stress indicated by cracking during growth could certainly cause the low strengths observed. Residual stress levels can be reduced by annealing or, possibly, by flattening the solidification interface with modified growth conditions. Alternatively, the strength controlling flaws may result from compositional gradients as has been previously observed for unusually weak single-crystal YAG monofilaments grown by the EFG process (Ref. 8). Based on past experience, the present monofilaments should exhibit more typical strength levels when the problem is identified and corrected.

Coefficient of Thermal Expansion

The average coefficient of thermal expansion (CTE) measured for polycrystalline $Y_2Ti_2O_7$ (23-1000°C) was 11.21 x 10^{-6} $°C^{-1}$. Experimental data are shown in Figure 15. Derivative values increased slightly with increasing temperature over this range. As was anticipated, the CTE is higher than those of alumina and spinel. The CTE is approximately the same as that of TiAl and provides a better match than either alumina or spinel to orthorhombics as well as other important aluminides such as Ti_3Al.

Chemical Compatibility of $Y_2Ti_2O_7$ Monofilaments With Titanium-Based Matrices

Figure 16 shows a scanning electron micrograph of the monofilament/matrix alloy interface for a [111] orientation $Y_2Ti_2O_7$ monofilament in a beta alloy (Alloy C) matrix in the as-hot-pressed condition and the results for multiple chemical analysis points both internal and external to the monofilament. (Oxygen is not detected accurately with this instrument so only metals are reported and normalized to 100%.) The SEM photomicrograph shows that the [111] orientation monofilament is subject to damage by cutting and polishing for metallographic specimen preparation. The

analysis points 1 and 2 show the composition of the phases observed in the matrix alloy. Points 3, 4, and 5, which are in the monofilament, show identical Y/Ti ratios. The contrast shown near the edge of the monofilament (point 3) suggests that the monofilament is exchanging oxygen with the matrix alloy but no chemical reaction (i.e., creation of new phases) is occurring at the matrix alloy/monofilament interface.

Figure 17 shows a similar interface between a [111] orientation $Y_2Ti_2O_7$ monofilament and an orthorhombic matrix along with the location of six analysis points. Note again that points 1, 2, and 3, inside the monofilament, show a constant Y/Ti ratio indicating no chemical reaction at the interface. Points 5 and 6 show the composition of the two phases present in the matrix alloy. The contrasting ring at the edge of the monofilament suggests some oxygen exchange with the matrix alloy but much less than observed for the Alloy C matrix.

Figure 18 shows the interface between a [311] orientation $Y_2Ti_2O_7$ monofilament and an α-2 matrix alloy along with the location of five analysis points. Points 4 and 5, in the monofilament, show a constant Y/Ti ratio, again confirming no chemical reactions have occurred. No contrasting ring is observed near the monofilament surface, suggesting little if any oxygen exchange with the matrix alloy (which in turn suggests that the stoichiometry of the [311] orientation monofilaments may be different from the [111] orientation monofilaments). Also, the [311] orientation monofilaments were much less damaged by cutting and polishing for metallography than the [111] orientation monofilaments.

As another check of matrix alloy/monofilament chemical interactions, a micro-hardness survey was made across the monofilament and at 0.025 in. intervals into the matrix alloy starting at the edge of the monofilament. The results are shown in Table 4 and appear to confirm the absence of any matrix alloy/monofilament chemical interaction.

Table 4. Microhardness Traverse Across Matrix Alloy/Monofilament Interface

Location	DPH Microhardness (15 g load)
Filament core	2406, 2406
Filament edge	1739, 1655
Matrix edge	424
Matrix edge +0.025 in.	435
Matrix edge +0.050 in.	435
Matrix edge +0.075 in.	424
Matrix edge +0.100 in.	424
Matrix edge +0.125 in.	435

For similar hot pressing conditions, 1/3 of a single-crystal sapphire monofilament is consumed by chemical interaction. Although it has not yet been determined whether the ≈1 μm thick band at the monofilament/matrix interface is a gap resulting from CTE mismatch (matrix ≈ 9 x 10^{-6} $°C^{-1}$) or is a polishing artifact, it is evident that the monofilament was not attacked during hot pressing. Monofilament pushout and more complete interface characterizations are needed to confirm initial favorable observations about chemical compatibility.

CONCLUSIONS

These first evaluations of $Y_2Ti_2O_7$ show that this material has several attributes which make it a potential reinforcement for Ti-alloy and Ti-intermetallic composites. Interfaces between these monofilaments and candidate Ti-based matrices indicate that the anticipated thermochemical compatibility was realized at least during the very demanding conditions used for hot pressing. Also, the thermal expansion coefficient is higher than those of other investigated oxide reinforcements, providing a better match to the relatively high values exhibited by important structural aluminides, including Ti_3Al, orthorhombics, and TiAl. Tensile strengths of the monofilaments are deficient at this point. Once factors responsible for the unusual, large internal flaws are identified and these flaws are eliminated, $Y_2Ti_2O_7$ monofilaments are expected to exhibit more typical strengths and the superior high temperature mechanical properties anticipated for this material on the basis of crystal structure should be realized. Although growth is more complex for $Y_2Ti_2O_7$, than for simple oxides, it was found that single-crystal monofilaments can be produced with selectable growth axes from well behaved melts in the laser-heated floating zone process.

REFERENCES

1. J.S. Haggerty and W.P. Menashi, "Production of Oxide Monofilaments by a Floating Zone Monofilament Drawing Technique," NASA, Contract No. NAS 3-13479, February 1971.

2. E.L. Courtright, J.S. Haggerty, and J. Sigalovsky, "Controlling Microstructures in $ZrO_2(Y_2O_3)$-Al_2O_3 Eutectic Monofilaments," Ceram. Eng. Sci. Proc. **14** [7-8] , 671-681 (1993).

3. Phase Diagrams for Ceramists, Vol. 6, Ed. R.S. Roth, J.R. Dennis, H.F. McMurdie. American Ceramic Society, 1987, Fig. 6502, p. 181.

4. W.J. Becker and G. Will, "Zur Kristallstruktur von $Y_2O_3 \cdot 2TiO_2$," Z. Naturforsch, **24B**, 259 (1969).

5. W.J. Becker and G. Will, "Roentgen-und Neutronenbeugungsuntersuchungen an $Y_2Ti_2O_7$," Z. Kristallogr., **131** 278-288 (1970).

6. JCPDS File 42-0413 (1991).

7. J.E. Sheehan, J. Sigalovsky, J.S. Haggerty, and J.R. Porter, "Mechanical Properties of $MgAl_2O_4$ Single-crystal Monofilaments," Ceram. Eng. Sci. Proc. **14** [7-8] 660-670 (1993).

8. G.S. Corman, General Electric Co., Schenectady, NY, private communication (1996).

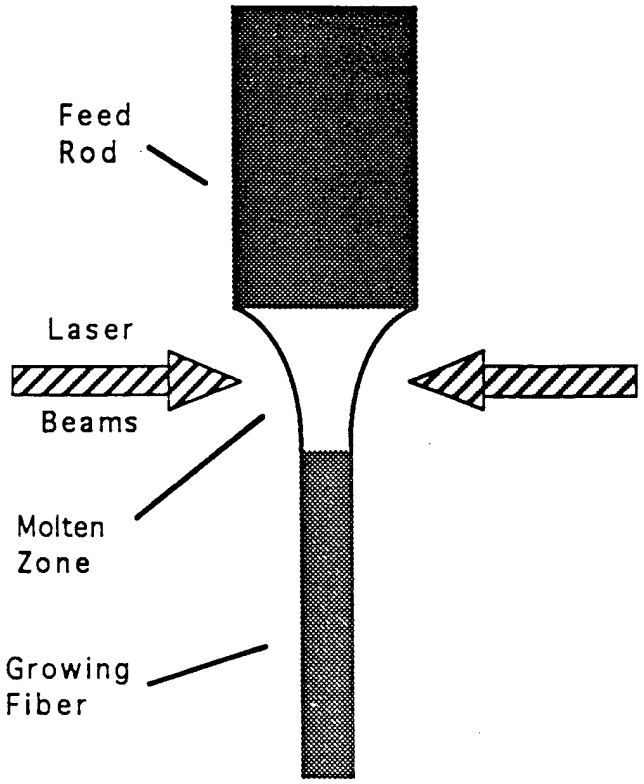

Figure 1. Laser-heated floating-zone monofilament growth schematic.

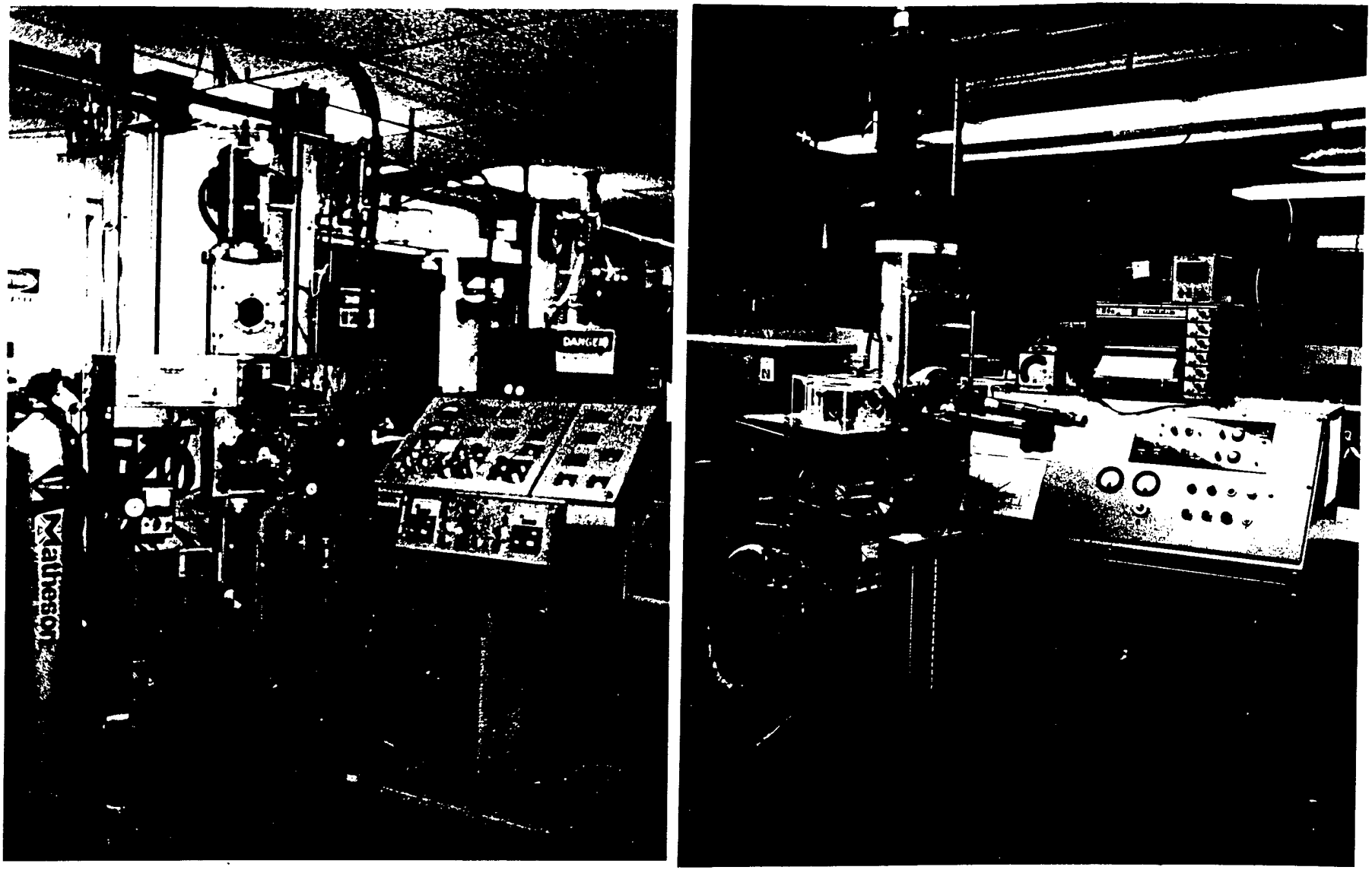

(a) (b)

Figure 2. Laser heated floating zone (LHFZ) monofilament growth units at MIT. (a) 1500 watt CO_2 laser with 4-beam optics, (b) 1500 watt CO_2 laser with 2-beam optics.

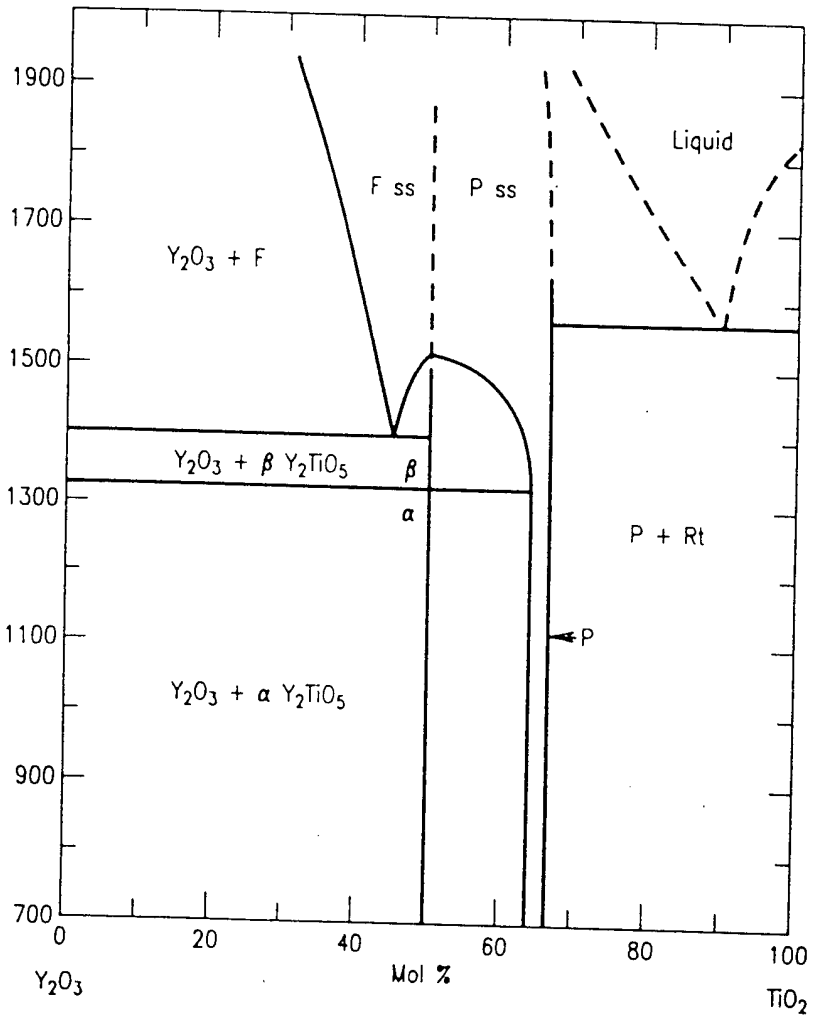

Figure 3. Y_2O_3 - TiO_2 phase diagram. F = fluorite, Rt = rutile, P = pyrochlore.

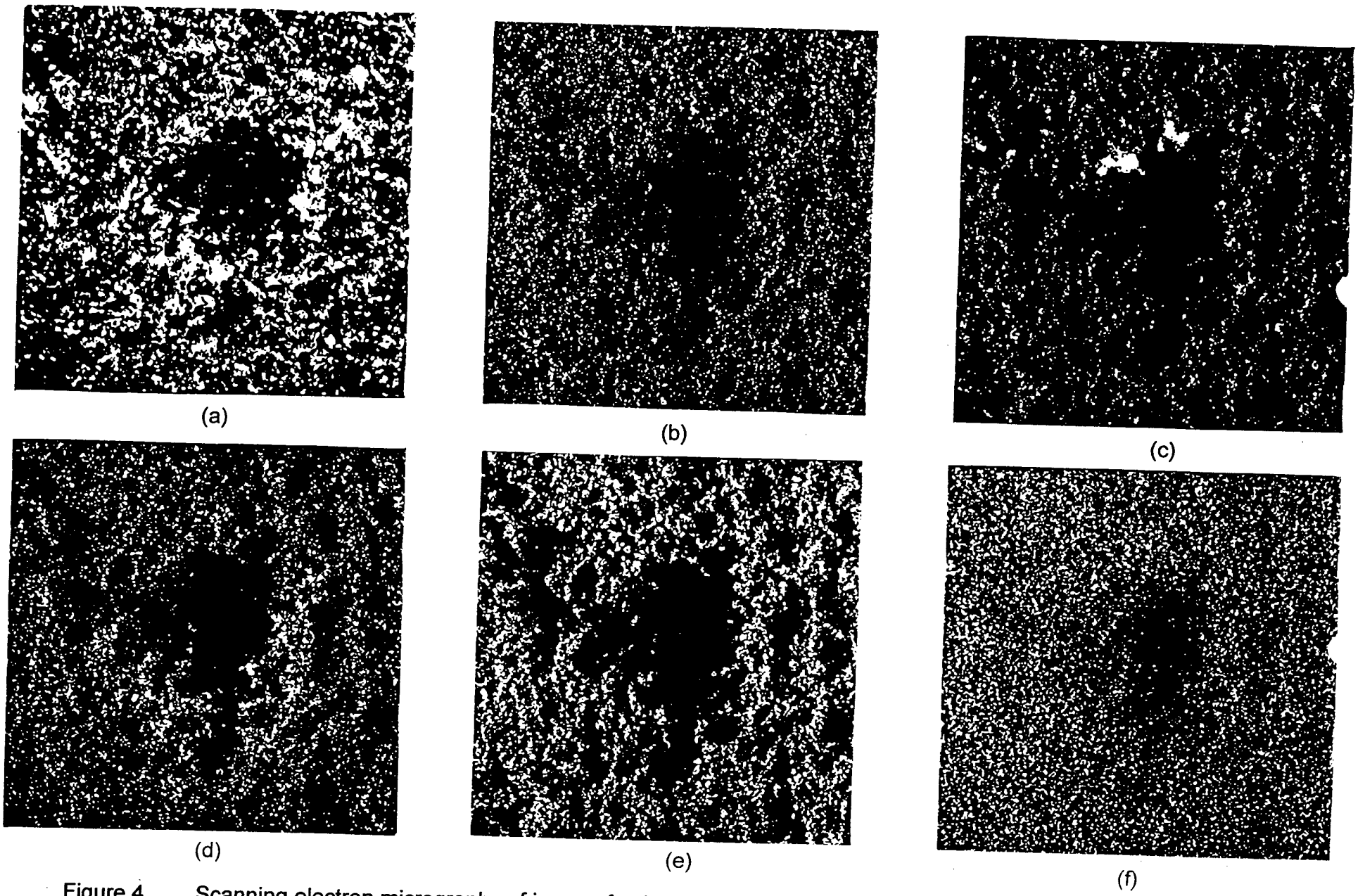

Figure 4. Scanning electron micrographs of impure feed rod dark spot. (a) image, (b) x-ray scattering background, (c) Al map, (d) Fe map, (e) Ti map, (f) Y map.

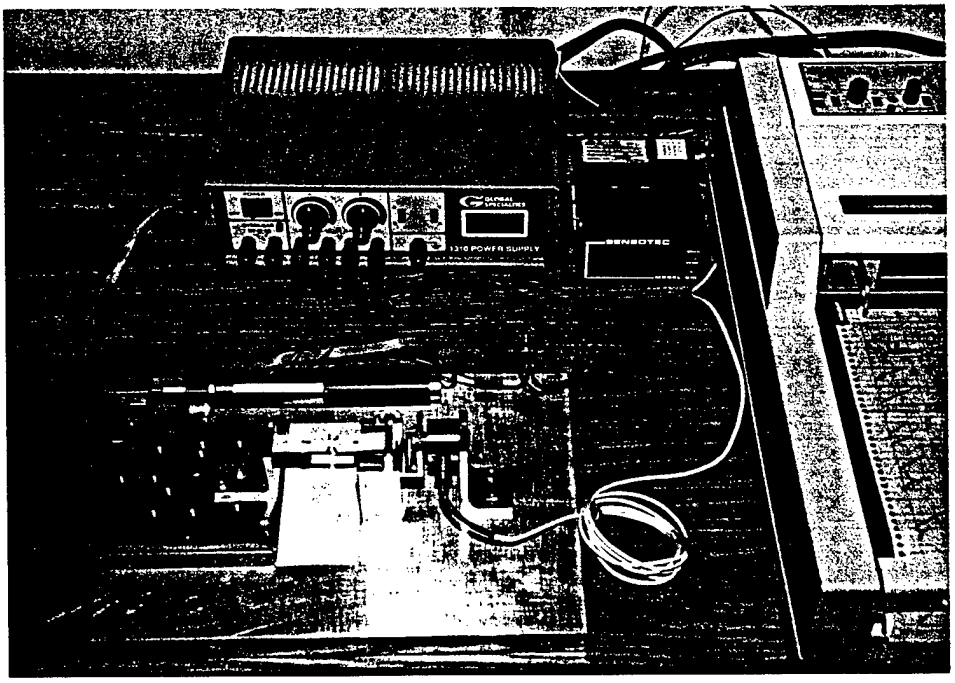

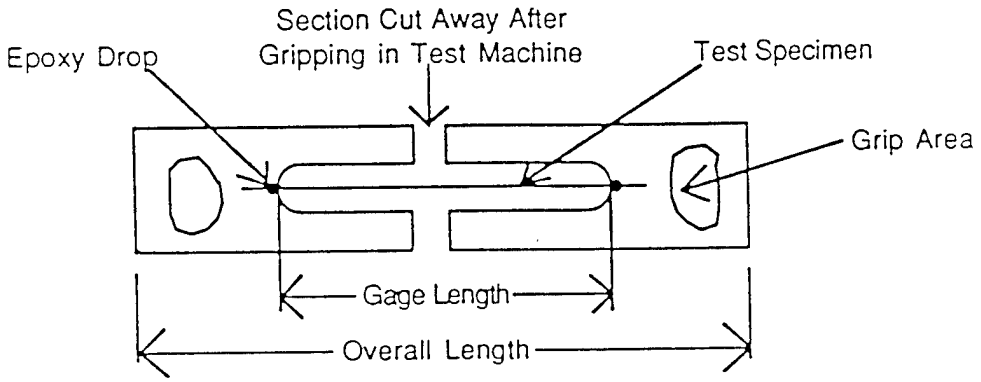

Figure 5. Photograph of monofilament tensile testing device and schematic of fiber mounting for tensile testing.

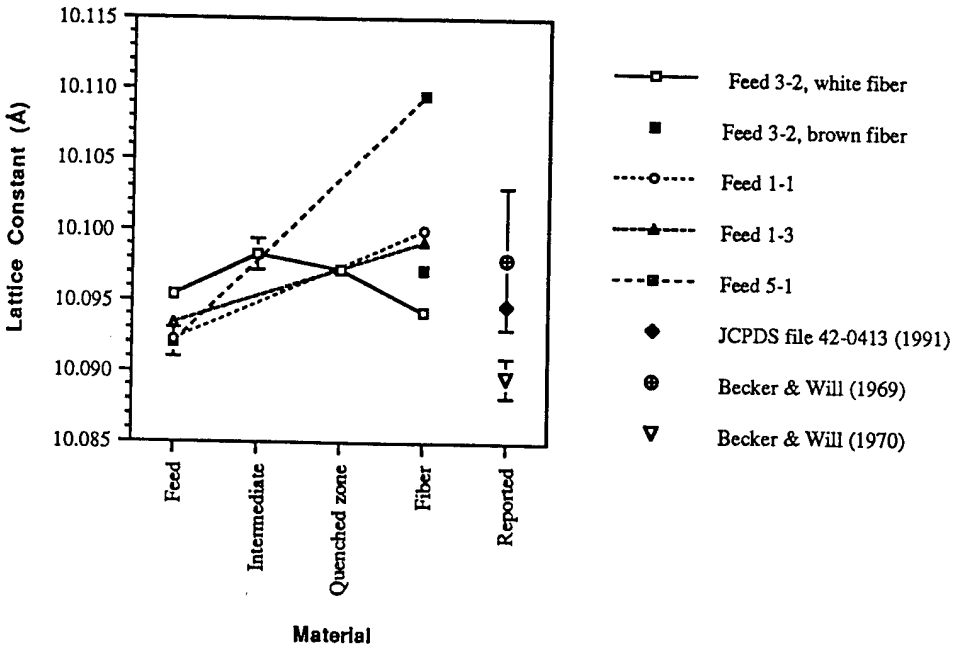

Figure 6. $Y_2Ti_2O_7$ lattice parameter evolution during growth.

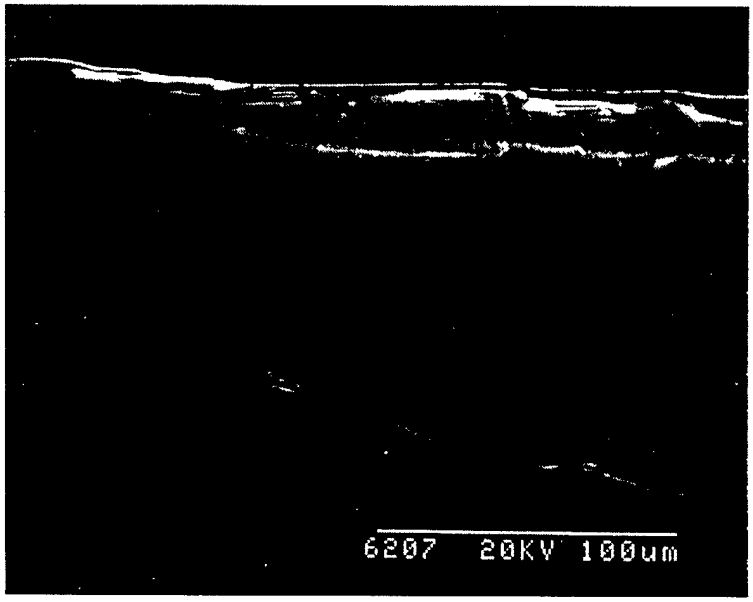

Figure 7. Large flat surface facets on [311] monofilament grown at 10 cm/h.

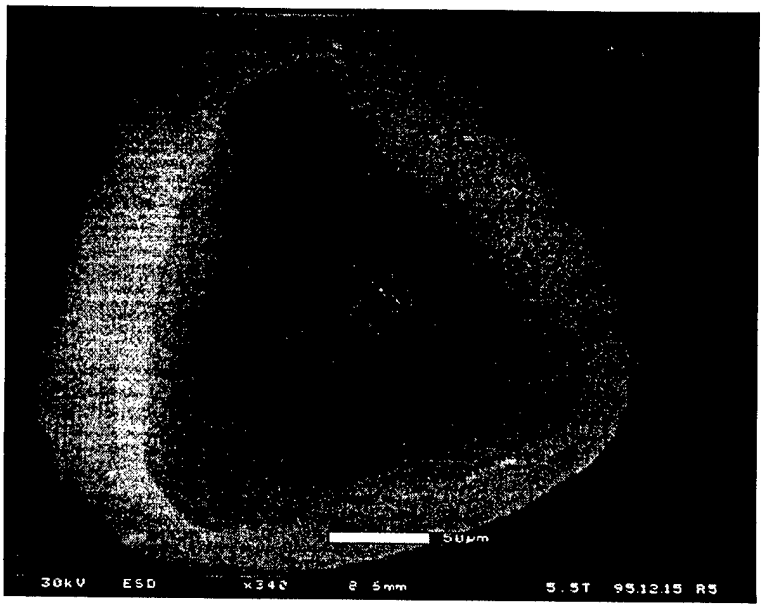

Figure 8(a). SEM micrograph of (a) axial view of triangular shaped [111] monofilament grown at 10 cm/h, 340X.

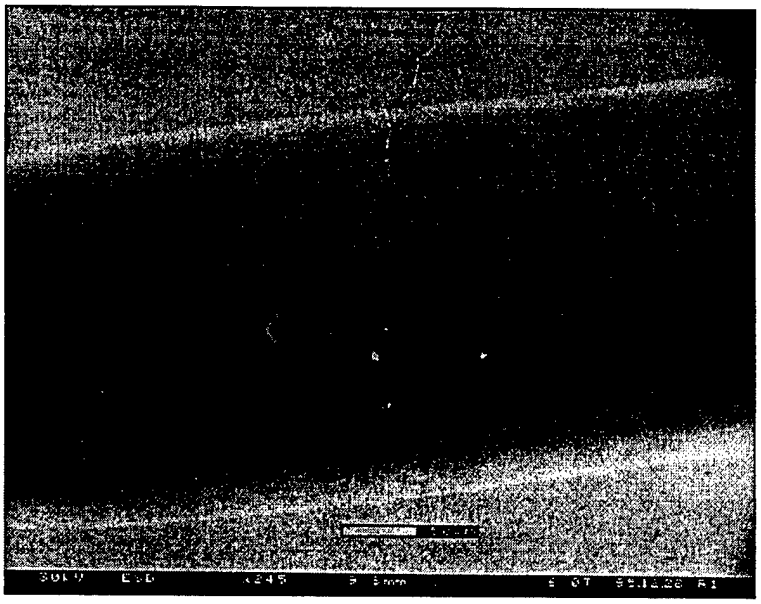

Figure 8(b). SEM micrograph of typical {211} face, 245X.

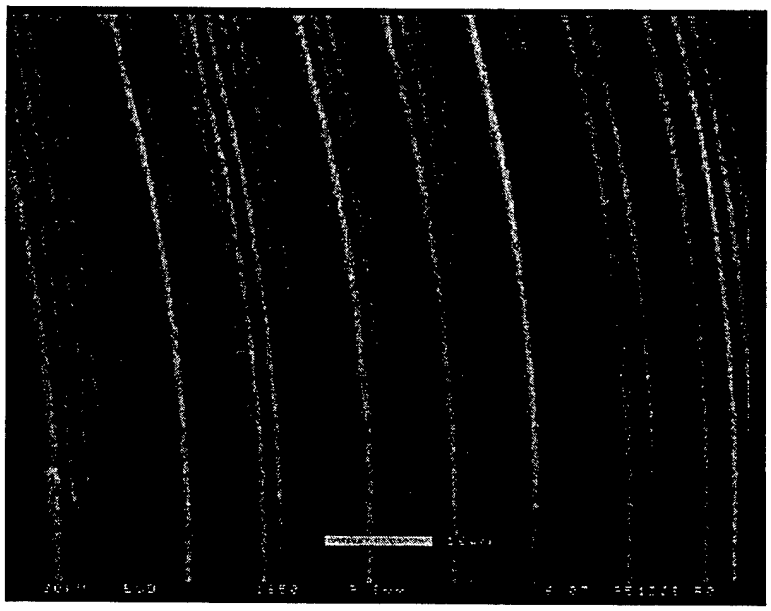

Figure 8(c). SEM micrograph of same {211} face shown in (b), 1850X.

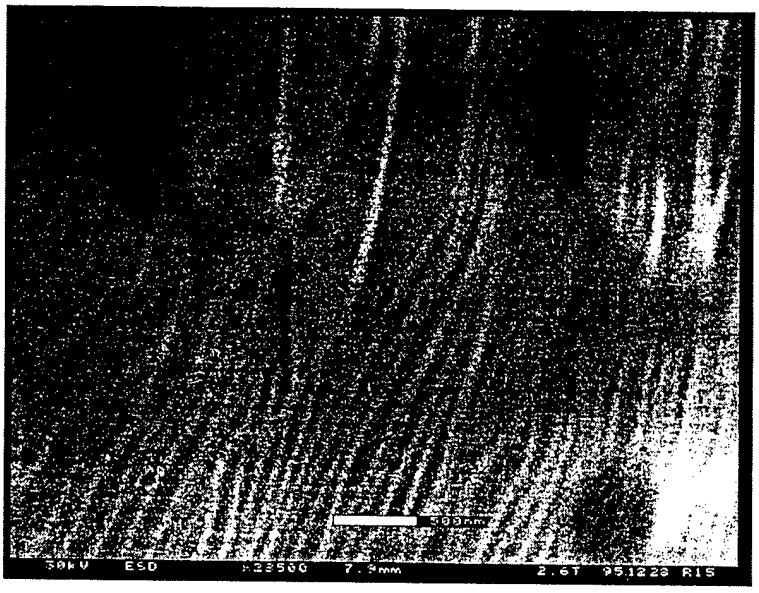

Figure 8(d). SEM micrograph of same {211} face shown in (b), 28,500X.

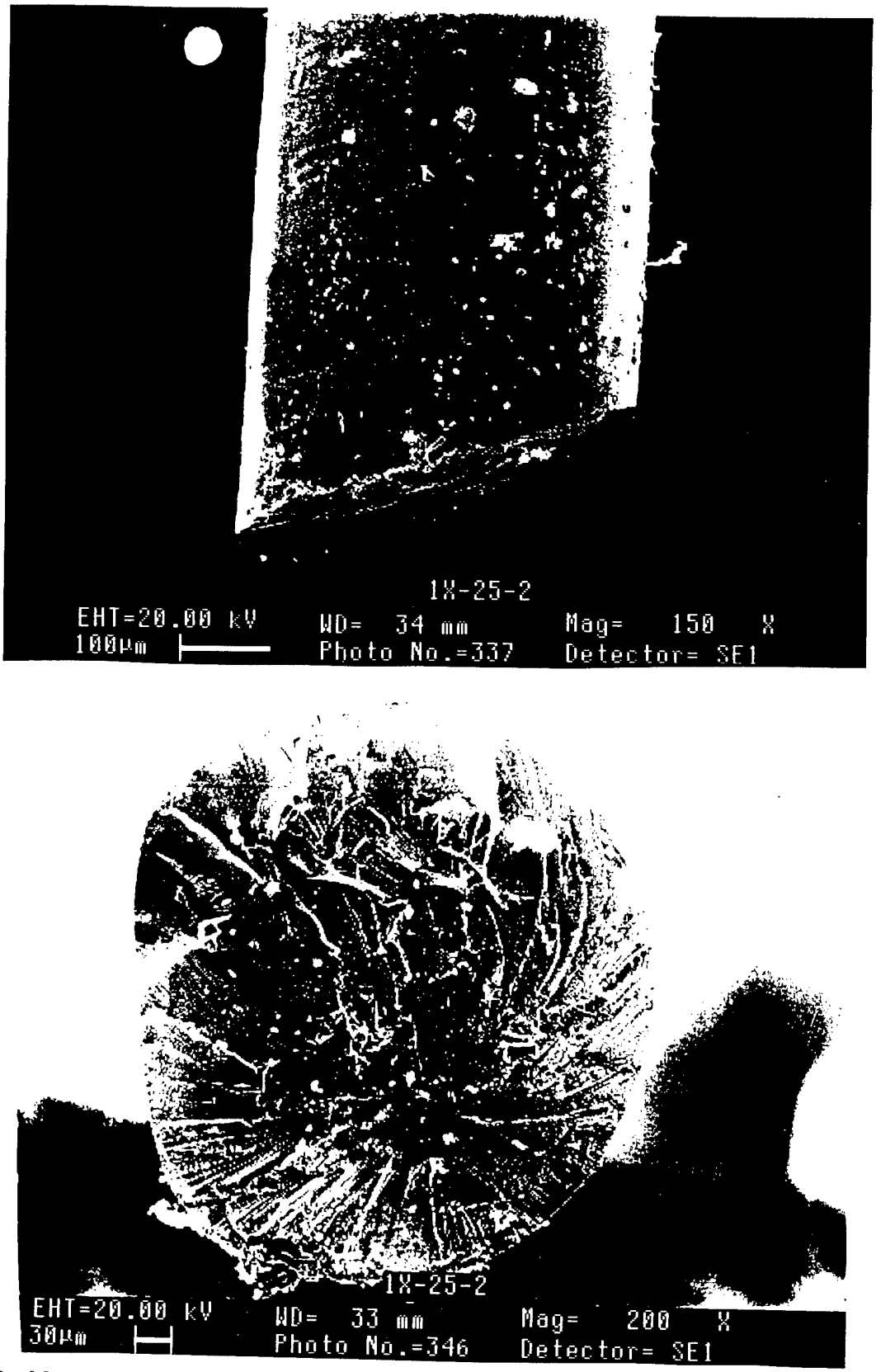

Figure 9. Monofilament surface (top) and fracture surface from tensile test (bottom) for $Y_2Ti_2O_7$ monofilament specimen No. 1X-25-2, [311] axis, as grown. Magnification: top, 150X; bottom, 200X.

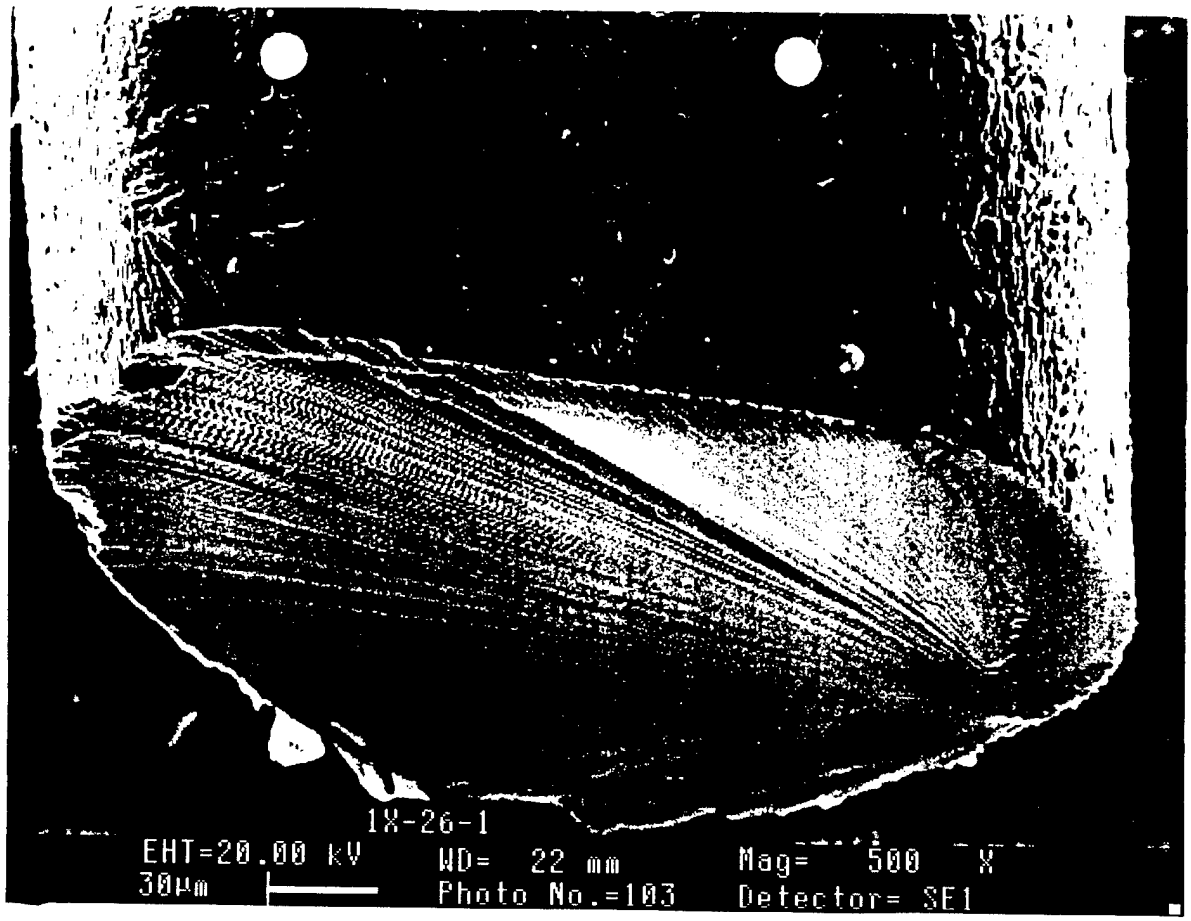

Figure 10. Monofilament surface (top) and fracture surface from tensile test (bottom) for $Y_2Ti_2O_7$ monofilament specimen No. 1X-26-1, [311] axis, annealed at 1300°C for 100 h in air. Magnification: top, 500X; bottom, 300X.

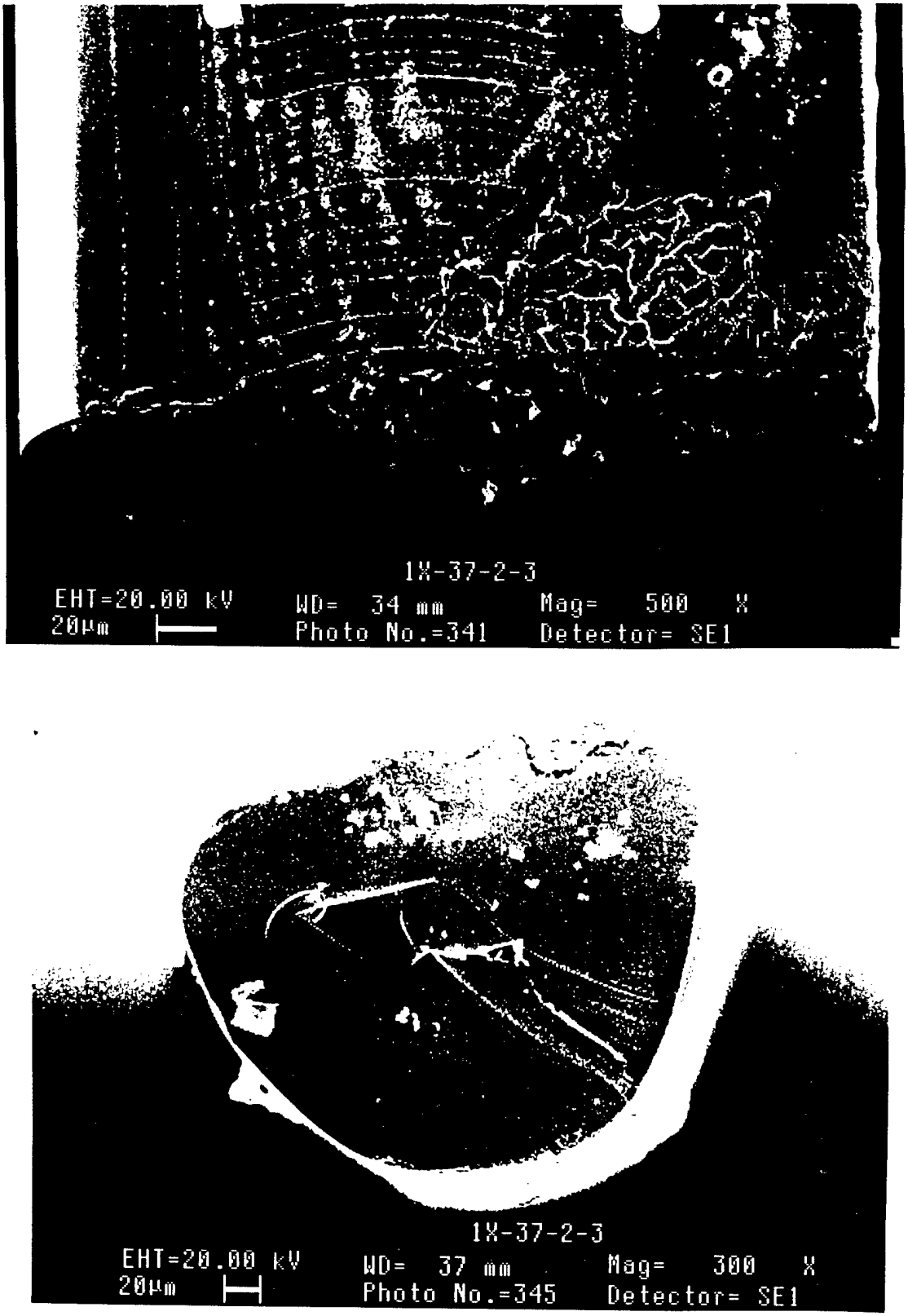

Figure 11. Monofilament surface (top) and fracture surface from tensile test (bottom) for $Y_2Ti_2O_7$ monofilament specimen No. 1X-37-2-3, [111] axis, as grown. Magnification: top, 500X; bottom, 300X.

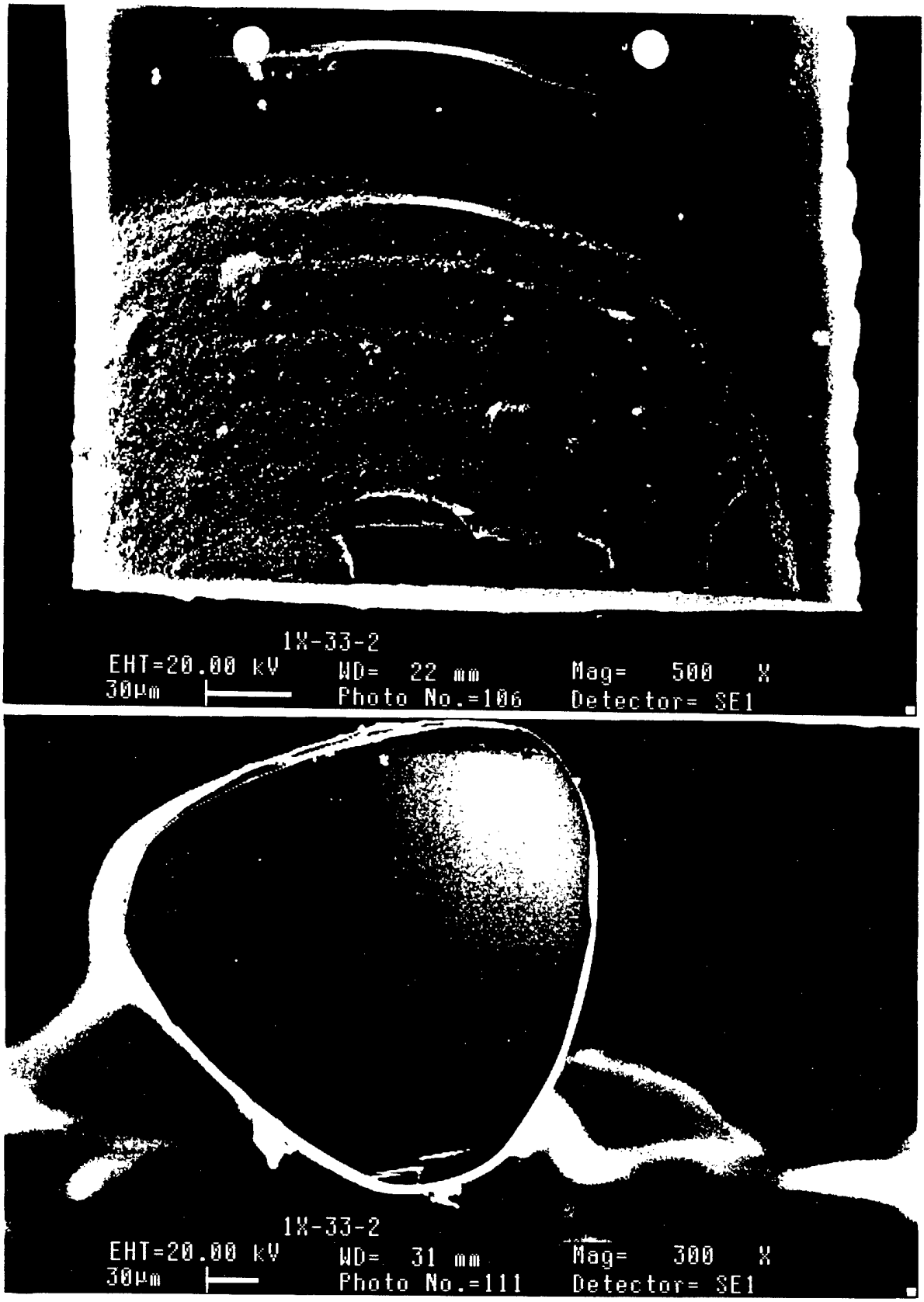

Figure 12. Monofilament surface (top) and fracture surface from tensile test (bottom) for $Y_2Ti_2O_7$ monofilament specimen No. 1X-33-2, [11.1] axis, as grown. Magnification: top, 500X; bottom, 300X.

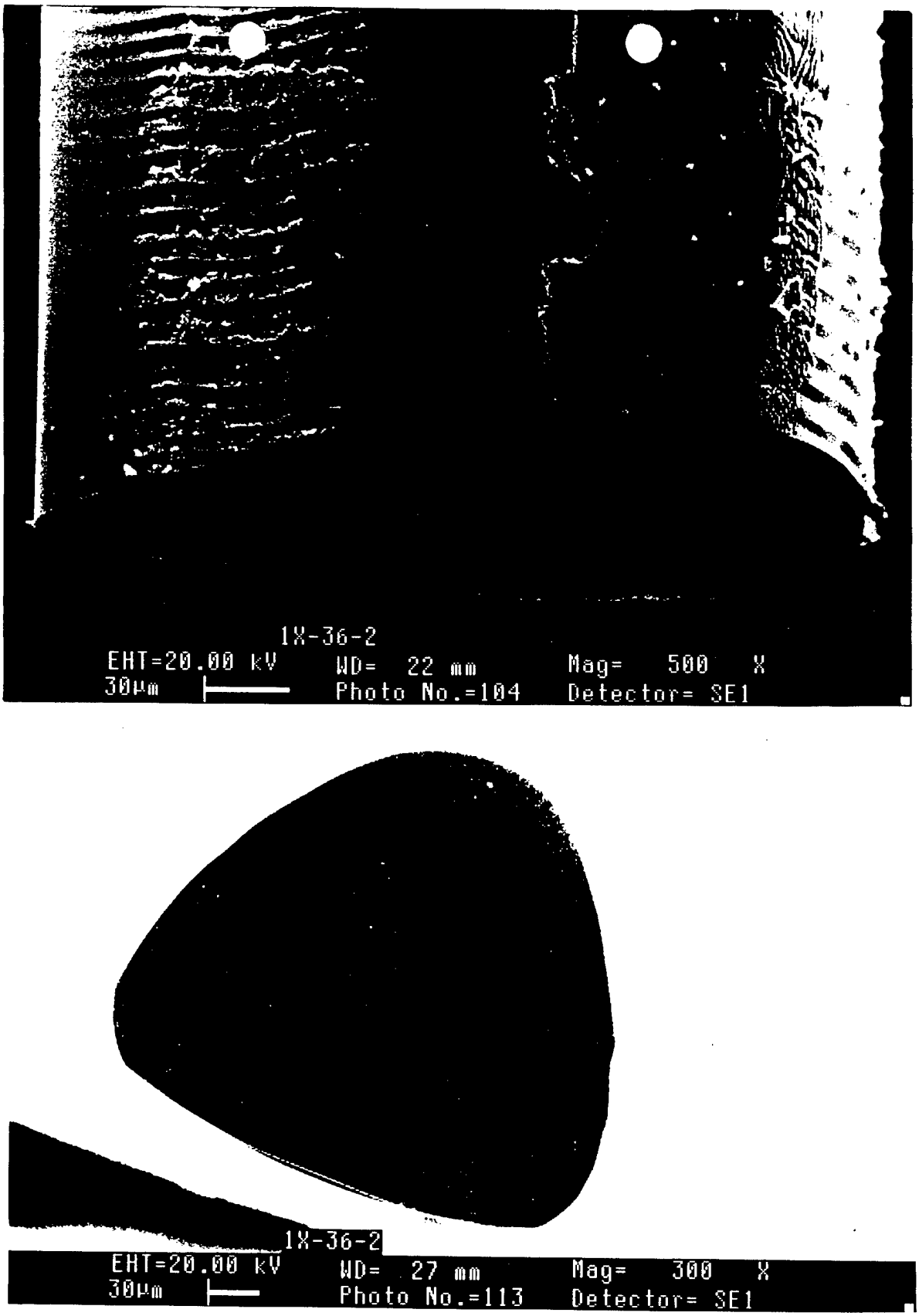

Figure 13. Monofilament surface (top) and fracture surface from tensile test (bottom) for $Y_2Ti_2O_7$ monofilament specimen No. 1X-36-2, [111] axis, as grown. Magnification: top, 500X; bottom, 300X.

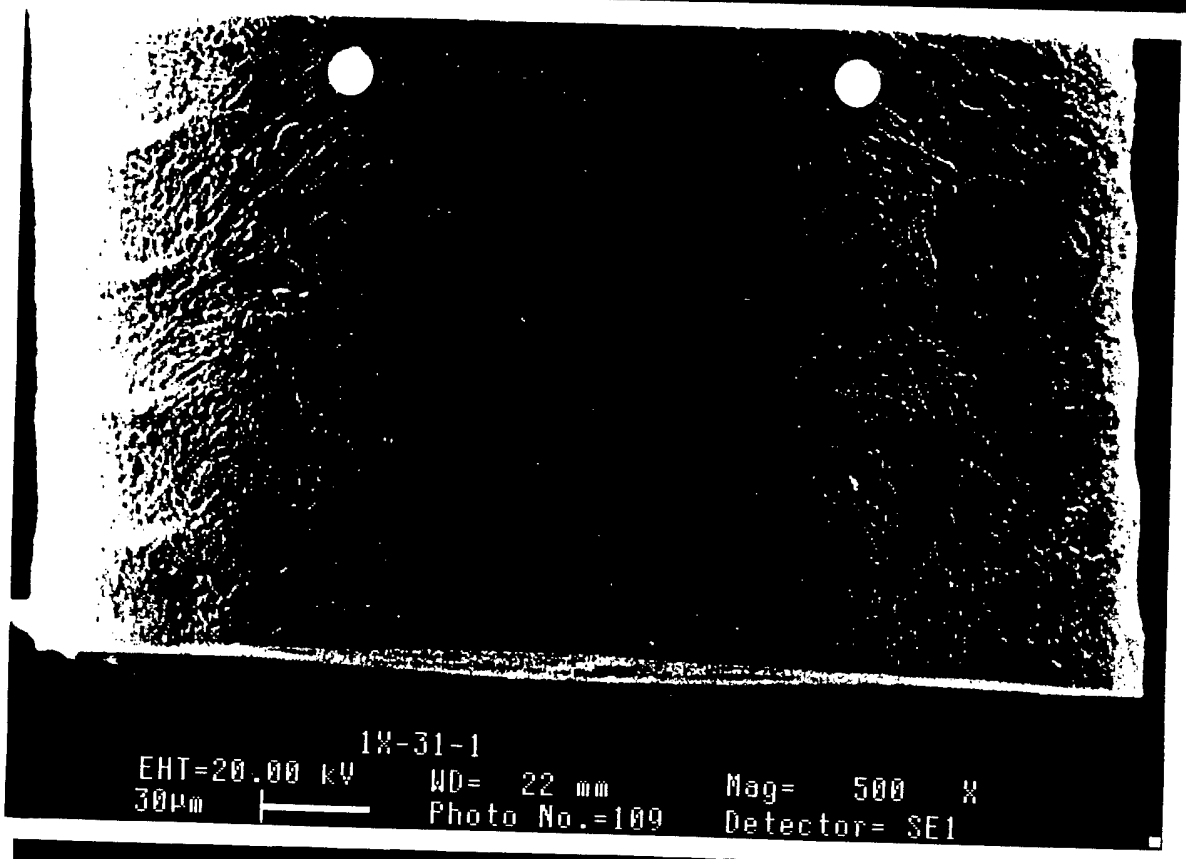

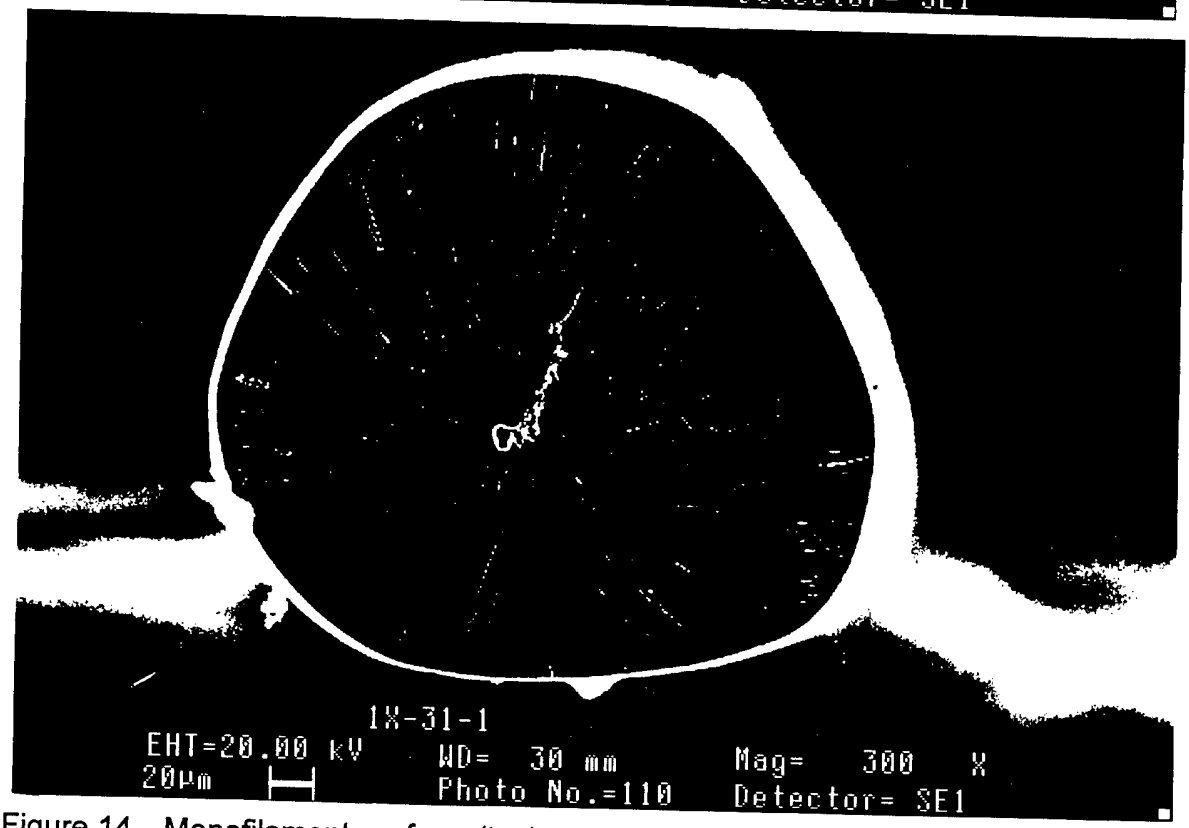

Figure 14. Monofilament surface (top) and fracture surface from tensile test (bottom) for $Y_2Ti_2O_7$ monofilament specimen No. 1X-31-1, [111] axis, annealed at 1300°C for 100 h in air. Magnification: top, 500X; bottom, 300X.

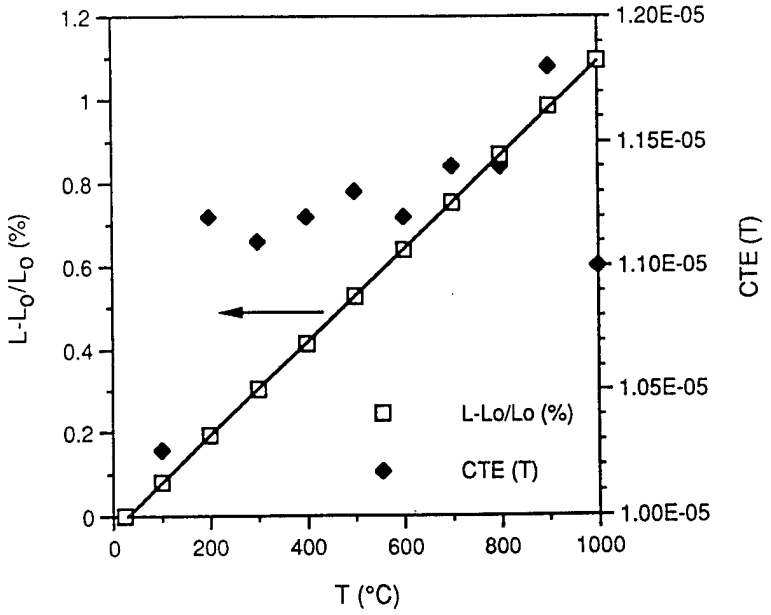

Material	CTE x 10^{-6} ($°C^{-1}$)
Beta Alloys (Ti-Cr-V)	7.5
α-2 (Ti_3Al)	9.0
Orthorhombic (Ti_2AlNb)	9.5
Gamma (TiAl)	11.5
$Y_2Ti_2O_7$	11.0

Figure 15. Coefficient of thermal expansion (CTE) of $Y_2Ti_2O_7$ and relative expansion coefficients of candidate matrix alloys.

Atom %

Point No.	Y	Ti	Al	Cr	V
1	0.1	35.8	0.2	18.7	45.2
2	-	90.3	0.1	2.2	7.5
3	57.3	41.5	1.0	-	0.3
4	57.6	41.1	1.2	-	0.2
5	57.2	41.5	0.9	0.1	0.3

Figure 16. Top, scanning electron micrograph of $Y_2Ti_2O_7$ monofilament in Alloy C matrix showing locations of analysis points. Bottom, results of x-ray analyses.

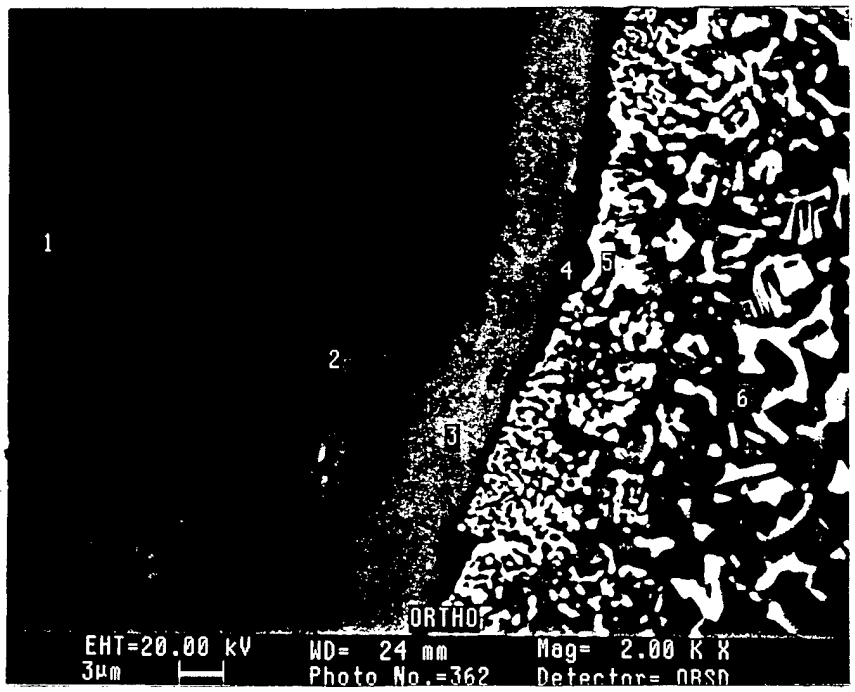

Atom %

Point No.	Y	Ti	Al	Cr	V
1	58.2	40.5	1.2	-	0.1
2	57.8	40.8	1.3	-	0.1
3	57.9	40.7	1.4	-	-
4	4.0	94.2	0.9	0.9	-
5	-	40.7	16.0	43.3	0.1
6	-	62.2	19.9	17.9	-

Figure 17. Top, scanning electron micrograph of $Y_2Ti_2O_7$ monofilament in an orthorhombic matrix showing locations of analysis points. Bottom, results of x-ray analyses.

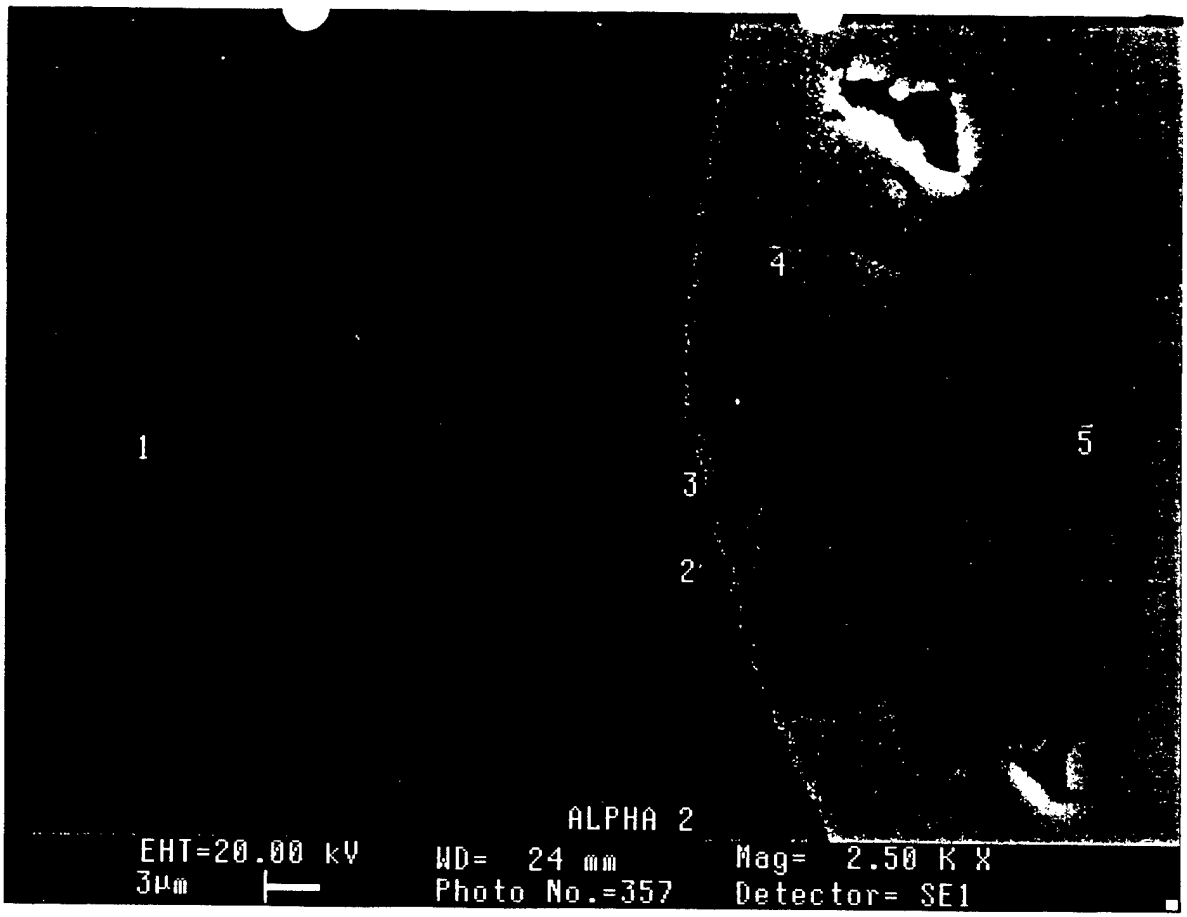

Atom %

Point No.	Y	Ti	Al
1	0.1	57.1	42.8
2	0.6	68.1	31.3
3	23.1	24.8	52.1
4	56.9	41.7	1.3
5	57.6	41.3	1.2

Figure 18. Top, scanning electron micrograph of $Y_2Ti_2O_7$ monofilament in an α-2 matrix showing locations of analysis points. Bottom, results of x-ray analyses.